RESEARCH PAPER

Tunable optofluidic microlens through active pressure control of an air–liquid interface

Jinjie Shi · Zak Stratton · Sz-Chin Steven Lin · Hua Huang · Tony Jun Huang

Abstract We demonstrate a tunable in-plane optofluidic microlens with a 9× light intensity enhancement at the focal point. The microlens is formed by a combination of a tunable divergent air–liquid interface and a static polydimethylsiloxane lens, and is fabricated using standard soft lithography procedures. When liquid flows through a straight channel with a side opening (air reservoir) on the sidewall, the sealed air in the side opening bends into the liquid, forming an air–liquid interface. The curvature of this air–liquid interface can be conveniently and predictably controlled by adjusting the flow rate of the liquid stream in the straight channel. This change in the interface curvature generates a tunable divergence in the incident light beam, in turn tuning the overall focal length of the microlens. The tunability and performance of the lens are experimentally examined, and the experimental data match well with the results from a ray-tracing simulation. Our method features simple fabrication, easy operation, continuous and rapid tuning, and a large tunable range, making it an attractive option for use in lab-on-a-chip devices, particularly in microscopic imaging, cell sorting, and optical trapping/manipulating of microparticles.

Keywords Optofluidic · Tunable lens · Microfluidics · Air–liquid interface

J. Shi · Z. Stratton · S.-C. S. Lin · H. Huang · T. J. Huang (✉)
Department of Engineering Science and Mechanics,
The Pennsylvania State University, University Park,
PA 16802, USA
e-mail: junhuang@psu.edu

1 Introduction

Adaptive optical systems are critical in a variety of on-chip biological/chemical assays, including sensing (Levy and Shamai 2007; Zourob et al. 2005; Shi et al. 2007; Shi et al. 2008a), microscopic imaging (Sinton et al. 2003; Heng et al. 2006; Cui et al. 2008; Wu et al. 2008), cell sorting (Wang et al. 2005), particle manipulation (Monneret et al. 2007; Shi et al. 2008b; Blakely et al. 2008), and single-particle detection/analysis (Yin et al. 2007; Hunt and Wilkinson 2008; Yang et al. 2009; Mao et al. 2009a). However, most optical systems are currently made with solid materials (such as glasses, metals, and semiconductors) (Psaltis et al. 2006). It is challenging to miniaturize these solid optical systems and integrate them with other "lab-on-a-chip" components. Moreover, these solid optical systems have limited tunability. Whereas tremendous effort has been devoted to integrating multiple fluid-manipulating components (e.g., pumps, switches, valves) on-chip, most optical components necessary to complex lab-on-a-chip devices remain off-chip (Psaltis et al. 2006). The field of optofluidics, the combination of optics and microfluidics, offers advantages over solid optical systems (Psaltis et al. 2006; Horowitz et al. 2008). Such advantages include: convenience in changing the optical property by simply altering the liquids, more feasibility in system reconfiguration due to the unlimited deformability of liquids, and ease in device fabrication and system integration, enabled by soft-lithography and microelectromechanical system technologies. Thus, in the past decade there has been much research directed at developing optofluidic components such as light sources (Li et al. 2006; Shopova et al. 2007), detectors (Erickson et al. 2008), waveguides (Wolfe et al. 2004; Schmidt and Hawkins 2008; Lim et al. 2008), and switches (Domachuk et al. 2005; Groisman et al. 2008; Lapsley et al.

2009). Particular effort has been dedicated to the development of tunable microlenses due to the ubiquitousness of tunable lenses in optical systems (Chronis et al. 2003; Zhang et al. 2003; Godin et al. 2006; Baird et al. 2007; Rosenauer and Vellekoop 2009; Miccio et al. 2009a). Tunable microlenses can be sorted into two categories: those that focus light in the plane of the substrate (in-plane) and those that focus light perpendicular to the plane of the substrate (out-of-plane) (Groisman et al. 2008).

There are a large number of demonstrated out-of-plane tunable microlenses based on different mechanisms. A commonly used approach is to contain liquid with an elastic membrane and alter the curvature of the membrane by direct mechanical actuation (Ren and Wu 2007), hydraulic pressure (Chronis et al. 2003; Pang et al. 2004), or electromagnetic actuation (Lee and Lee 2007). Another approach is to manipulate the interface between immiscible fluids (i.e., water–oil, water–air); this can be done through a variety of methods, including electrowetting (Grilli et al. 2008; Kuiper and Hendriks 2004; Miccio et al. 2009b), redox surfactants (Lopez et al. 2005), and stimuli-responsive hydrogels (Dong et al. 2006). Out-of-plane tunable microlenses are useful for imaging systems, but they often have relatively complex fabrication procedures (Ren and Wu 2007; Kuiper and Hendriks 2004; Lee and Lee 2007; Dong et al. 2006). Furthermore, because their optical axes are perpendicular to their substrates, they require optical alignment between multiple device layers, making device assembly and integration a challenge. These drawbacks make out-of-plane tunable microlenses impractical for many lab-on-a-chip devices.

In-plane tunable microlenses that can be simply fabricated, readily tuned, and easily integrated with other microfluidic components are needed to achieve functional on-chip applications. To date, a handful of in-plane tunable lenses have been developed, including a hydrodynamic cylindrical lens (Mao et al. 2007), a liquid-core liquid-cladding (L^2) lens (Tang et al. 2008; Song et al. 2009; Seow et al. 2008), a liquid gradient refractive index (L-GRIN) lens (Mao et al. 2009b), and a liquid droplet interfacing air lens (Dong and Jiang 2007). The hydrodynamic cylindrical lens was generated by passing two co-injected miscible liquids of different refractive indices through a curved channel, causing one liquid to bow into the other. The L^2 lens was generated through a laminar flow of three liquid streams, with a high refractive index stream (core) sandwiched between two low refractive index streams (cladding). By changing the relative flow speed of the core and cladding streams, a 6-mm tunable focal length was demonstrated. In the L-GRIN lens, the diffusion of solute ($CaCl_2$) between side-by-side co-injected microfluidic laminar flows was utilized to establish a hyperbolic secant (HS) refractive index profile to focus and

swing the light. In this work, we demonstrate an optofluidic microlens, fabricated via standard soft lithography protocol, which achieves variable focusing of light by means of active pressure control of an air–liquid interface. The liquid droplet interfacing air lens takes the advantage of the surface tension at microscale to form stable droplets inside a microfluidic channel. Through pneumatic control of the droplet in a microfluidic channel, the microlens can be tuned in focal length and moved in the channel on demand, thus achieving high reconfiguration.

2 Working mechanism

The working mechanism of the microlens is shown in Fig. 1. Deionized (DI) water is introduced into a straight microchannel. The microchannel makes a T-junction with an air reservoir. As the water flows past the T-junction, a quantity of air is trapped in the air reservoir and a movable air–water interface is formed at the T-junction (Fig. 1a), with the air bending into the water due to the air–liquid contact angle and the hydrophobic–hydrophilic interaction between the surface and liquid (Ahmed et al. 2009a, b; Tovar and Lee 2009). The refractive index of water is ∼1.33 and that of air is ∼1. Thus, the air–water interface acts as a divergent lens. A light beam from an optical fiber diverges when passing through the air–water interface, then converges when it encounters a static polydimethylsiloxane (PDMS) lens, consisting of PDMS polymer (refractive index ∼1.41) (Xia and Whitesides 1998) bending into an air gap. This PDMS lens causes the divergent incident light to converge to a focal point within the monitor chamber. The amount of divergence of the light incident on the PDMS lens determines the image distance (the distance between the PDMS lens apex and the light focal point) of the lens: the more the divergence, the longer the image distance.

When the flow rate of the DI water in the straight microchannel is increased, it applies increased pressure to the air–water interface, resulting in an increase in the interface's radius of curvature and an increase in the distance between the interface and PDMS lens (Fig. 1b–e). According to the Gaussian Optics Equation using the paraxial approximation (Hecht 2001), an increase in the radius of curvature of a divergent interface causes less divergence of the incident light. But when the interface moves away from the PDMS lens, it generates more divergence in the light reaching the PDMS lens. Thus, the increase in radius of curvature and the movement of the interface have counteracting effects on the amount of divergence in the light incident on the PDMS lens. However, the radius of curvature of the interface has a much stronger effect on the light divergence than the movement of the interface.
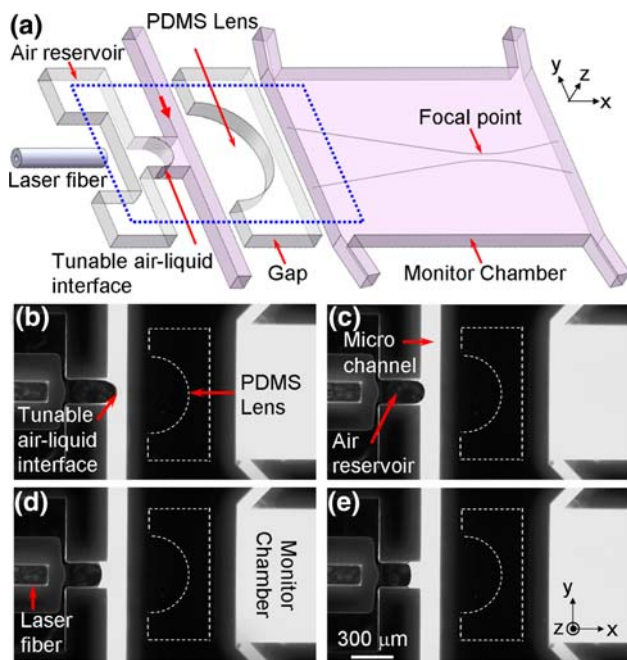
Fig. 1 **a** Schematic of the tunable lens. **b–e** Optical images of the device (region enclosed by the *dotted square* in **a**) taken at different flow rates of DI water in the microchannel: **b** 0 μL/min. **c** 20 μL/min. **d** 40 μL/min. **e** 60 μL/min. Liquid in the channel and monitor chamber is an aqueous solution of rhodamine fluorescent dye

Fig. 2 Optical image of the experimental microfluidic device. *Inset* (enclosed by the *dotted square*): zoom-in figure of the tunable lens

Therefore, as the flow rate of the DI water increases, the air–water interface generates less divergence in the light incident on the PDMS lens, resulting in a shorter image distance.

3 Device fabrication and system setup

The optofluidic microlens (Fig. 2) was fabricated from PDMS using standard soft lithography and mold-replica procedures (Xia and Whitesides 1998; Ahmed et al. 2009a, b; Shi et al. 2009a). First, a pre-patterned silicon wafer with photoresist was processed by deep reactive ion etching (DRIE, Adixen, Hingham, MA) to get the master mold. After the DRIE process, the silicon wafer was subsequently coated with 1H, 1H, 2H, 2H-perfluorooctyltrichlorosilane (Sigma–Aldrich) to reduce surface energy and hence the damage to the PDMS channel during the demolding process. This silanization step was critical because smooth channel sidewalls reduce scattering loss of incident light. Sylgard 184™ Silicone Elastomer base and curing agent (Dow Corning, Midland, MI) were mixed at a 10:1 weight ratio, cast onto the silicon mold, and cured at 70°C for 30 min. After the PDMS was cured, it was cut and peeled from the mold. Inlets and outlets were drilled with a silicon carbide drill bit and the device was subsequently bonded onto a glass slide. Polyethylene tubes were then inserted

into the inlets and outlets to connect the device to syringe pumps (KDS 210, KD scientific, Holliston, MA). Device dimensions are: 155 μm depth for the channel, air reservoir, PDMS lens, and fiber holder; 150 and 300 μm widths for the straight channel and side channel, respectively; and 300 μm radius for the PDMS lens.

Incident light was supplied by a green laser diode (532 nm) coupled into an optical fiber (Ocean Optics, N.A. = .22 ± .02, core and outer diameters are 50 and 150 μm, respectively). The optical fiber was inserted into a fiber holder (155 μm × 155 μm) in the PDMS such that the fiber was along the optical axis of the PDMS lens and air–water interface. To visualize the light rays, DI water with rhodamine fluorescent dye was injected into the straight microchannel and the monitor chamber. The intensity of fluorescence is proportional to the intensity of incident light. The concentration of the dye in the monitor chamber liquid was sufficiently low such that the incident light could propagate through the liquid without being significantly attenuated or absorbed, while the intensity of the incident light was sufficiently low (5 mW) so as to avoid photobleaching of the dye during the experiment. The device operation was observed through an inverted fluorescent optical microscope (Nikon TE 2000U), and optical images were taken using a CCD camera (CoolSNAP HQ2, Photometrics, Tucson, AZ) and a Nikon color digital camera mounted on the front viewport of the microscope.

4 Results and discussion

Figure 3 shows the experimental results obtained at flow rates of 0, 10, 20, 30, and 40 μL/min. As the flow rate of the DI water is increased, the increased pressure on the

Fig. 3 Ray-tracing experiments to characterize the variable focal length and light intensity at different flow rates of DI water. **a** 0 μL/min. **b** 10 μL/min. **c** 20 μL/min. **d** 30 μL/min. **e** 40 μL/min. The relative intensity was plotted via ImageJ®. **f** Intensity plots along the *white lines* depicted in **a–e**, where the *solid curves* are the fittings to the experimental data
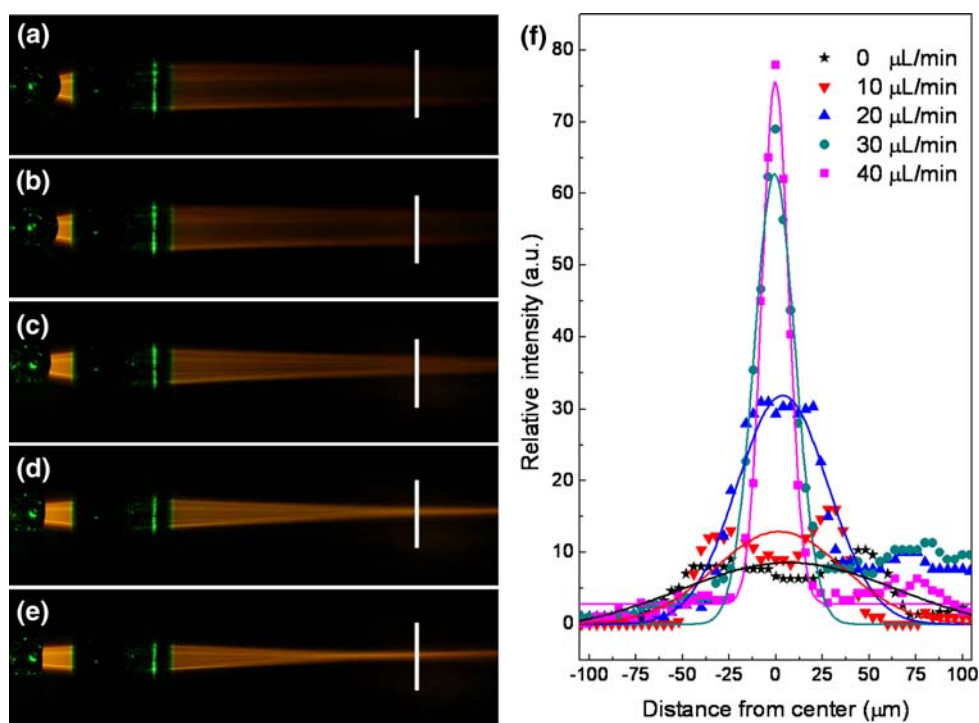
air–water interface flattens the interface and moves it away from the PDMS lens. As a result, the light focal point moves closer to the PDMS lens. With DI water as the injected liquid, a flow rate of 0 μL/min caused approximate collimation of the incident light, as shown in Fig. 3a and quantified in the graph of Fig. 3f. Subsequent increases in the flow rate caused gradual focusing of the light (Fig. 3b–e). A quantitative analysis (Fig. 3f) reveals that for a flow rate of 40 μL/min, the full width at half maximum (FWHM) of the focused beam is ∼20 μm, which is one-eighth of the original beam width. This FWHM value is comparable to the dimensions of most bioparticles, making

the lens applicable to single-cell detection and analysis (Yin et al. 2007; Yang et al. 2009; Mao et al. 2009a). The light intensity at the focal point (Fig. 3e) was ∼9 times the intensity of the collimated beam (Fig. 3a). The significant intensity enhancement generated by this lens may provide a method to use low-power lasers for on-chip dynamic particle trapping and manipulation, a process which normally requires high-power lasers (e.g., the laser intensity in optical tweezer-based manipulation is required to be $>10^9$ W/m^2) (Chiou et al. 2005).

To study the focusing properties of the tunable lens, a two-dimensional geometric ray-tracing program

Fig. 4 *Left* Fluorescence images of lens focusing, taken with a red filter to improve clarity, with corresponding (*right*) simulation results for flow speeds. **a** 0 μL/min. **b** 10 μL/min. **c** 15 μL/min. **d** 20 μL/min. **e** 25 μL/min. **f** 30 μL/min
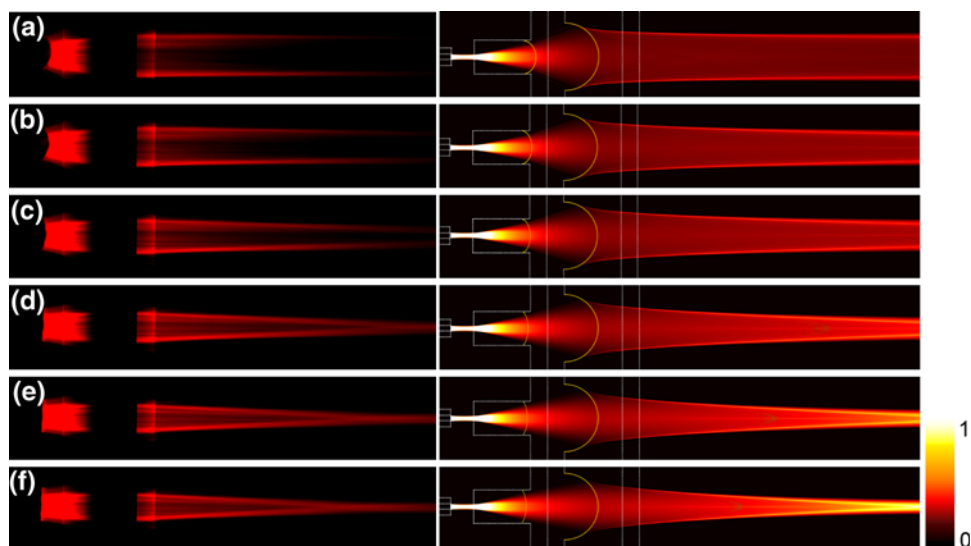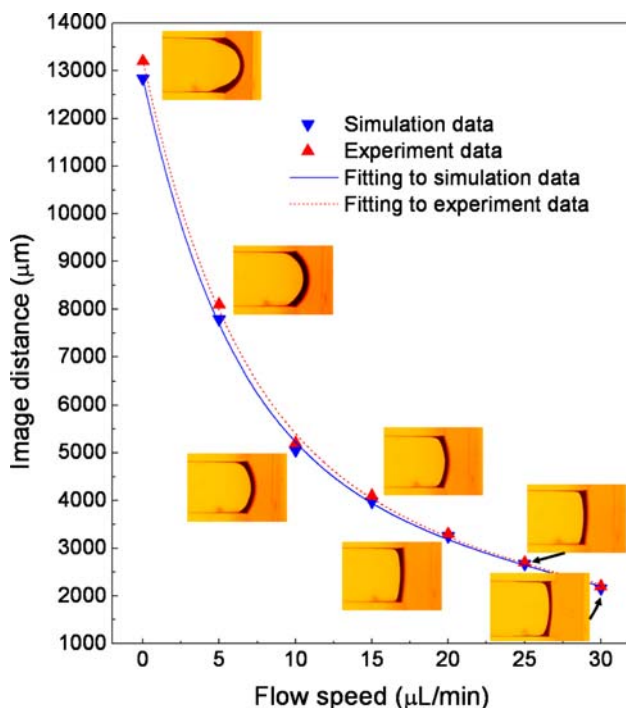
Fig. 5 The dependence of light focal length (measured from the apex of the PDMS lens to the focal point) on the flow rate of DI water in the straight microchannel (with *insets* showing the air–water interface curvature). Both simulated and experimental data sets are graphed, demonstrating strong congruence

(MATLAB® coding) was developed to simulate the propagation of light in the device. A Gaussian light source was defined at the opening of the optical fiber to emit rays of light. Snell's law was employed to calculate the refractive direction of each ray across interfaces of different materials along the light path. The curvatures of the air–liquid interface were extracted from experimental photographs at different flow rates and imported into the ray-tracing simulations. By summing the individual rays' powers, the light intensity distribution in the device was visualized as shown in Fig. 4. The simulation results (Fig. 4, right) match well with the experimental photographs (Fig. 4, left), strengthening the validity of the experimental results.

The congruence is quantified in Fig. 5, with lines fitted to the data points. As flow rate increases, the trapped air becomes increasingly more resistant to further compression, which explains the slope decrease of the fitted curve (Fig. 5). The data demonstrates that varying the liquid flow rate between 0 and 30 μL/min generates a tunable focal length of 11 mm. This relatively large tunable length makes the optofluidic microlens presented here a highly versatile option for on-chip imaging applications, such as confocal microscopy, where continuous scanning of the focal point is required.

5 Conclusions

In conclusion, we have demonstrated a tunable optofluidic microlens that focuses light in the plane of the device substrate. The microlens employs a static PDMS lens and an air–water interface that can be reshaped to tune the focal point of incident light. The interface is easily and stably reshaped by adjusting the flow rate of injected DI water. The microlens has a demonstrated tunable focal range of 11 mm, and brings incident light to a focal point with ∼9 times intensity enhancement, which compares favorably with other in-plane tunable lenses (the tunable focal lengths and intensity enhancements are: ∼1 mm and 1.5 times in Mao et al. 2007; ∼6.5 mm and 4.6 times in Tang et al. 2008; and 0.7 mm and 8 times in Mao et al. 2009b, respectively). The microlens is simply fabricated using standard soft lithography protocol and thus can be conveniently integrated with other microfluidic components. Although the microlens requires a continual flow of liquid to tune the image distance, the liquid remains pristine and thus can be recycled by looping the flow. Additional work must be done to realize the practical applications of this lens; we have projects underway to demonstrate use of the microlens in microscopic imaging applications and in dynamic optical trapping and manipulating of microparticles.

References

Ahmed D, Mao X, Shi J, Juluri BK, Huang TJ (2009a) A millisecond micromixer via single-bubble-based acoustic streaming. Lab Chip 9:2738–2741

Ahmed D, Mao X, Juluri BK, Huang TJ (2009b) A fast microfluidic mixer based on acoustically driven sidewall-trapped microbubbles. Microfluid Nanofluid 7:727–731

Baird E, Young P, Mohseni K (2007) Electrostatic force calculation for an EWOD-actuated droplet. Microfluid Nanofluid 3:635–644

Blakely JT, Gordon R, Sinton D (2008) Flow-dependent optofluidic particle trapping and circulation. Lab Chip 8:1350–1356

Chiou PY, Ohta AT, Wu MC (2005) Massively parallel manipulation of single cells and microparticles using optical images. Nature 436:370–372

Chronis N, Liu GL, Jeong KH, Lee LP (2003) Tunable microdoublet lens array. Opt Express 11:2370–2378

Cui X, Lee LM, Heng X, Zhong W, Sternberg PW, Psaltis D, Yang C (2008) Lensless high-resolution on-chip optofluidic microscopes for Caenorhabditis elegans and cell imaging. Proc Natl Acad Sci USA 105:10670–10675

Domachuk P, Cronin-Golomb M, Eggleton B, Mutzenich S, Rosengarten G, Mitchell A (2005) Application of optical trapping to beam manipulation in optofluidics. Opt Express 13:7265–7275

Dong L, Jiang H (2007) Tunable and movable liquid microlens in situ fabricated within microfluidic channels. Appl Phys Lett 91:041109

Dong L, Agarwal AK, Beebe DJ, Jiang H (2006) Adaptive liquid microlenses activated by stimuli-responsive hydrogels. Nature 442:551–554

Erickson D, Mandal S, Yang AHJ, Cordovez B (2008) Nanobiosensors: optofluidic, electrical and mechanical approaches to biomolecular detection at the nanoscale. Microfluid Nanofluid 4:33–52

Godin J, Lien V, Lo YH (2006) Demonstration of two-dimensional fluidic lens for integration into microfluidic flow cytometers. Appl Phys Lett 89:061106

Grilli S, Miccio L, Vespini V, Finizio A, Nicola SD, Ferraro P (2008) Liquid micro-lens array activated by selective electrowetting on lithium niobate substrates. Opt Express 16:8084–8093

Groisman A, Zamek S, Campbell K, Pang L, Levy U, Fainman Y (2008) Optofluidic 1 × 4 Switch. Opt Express 16:13499–13508

Hecht E (2001) Optics, Pearson Education, pp 159–161

Heng X, Erickson D, Baugh LR, Yaqoob Z, Sternberg PW, Psaltis D, Yang C (2006) Optofluidic microscopy—a method for implementing a high resolution optical microscope on a chip. Lab Chip 6:1274–1276

Horowitz VR, Awschalom DD, Pennathur S (2008) Optofluidics: field or technique? Lab Chip 8:1856–1863

Hunt HC, Wilkinson JS (2008) Optofluidic integration for microanalysis. Microfluid Nanofluid 4:53–79

Kuiper S, Hendriks BHW (2004) Variable-focus liquid lens for miniature cameras. Appl Phys Lett 85:1128–1130

Lapsley MI, Lin SCS, Mao X, Huang TJ (2009) An in-plane, variable optical attenuator using a fluid-based tunable reflective interface. Appl Phys Lett 95:083507

Lee SW, Lee SS (2007) Focal tunable liquid lens integrated with an electromagnetic actuator. Appl Phys Lett 90:121129

Levy U, Shamai R (2007) Tunable optofluidic devices. Microfluid Nanofluid 4:97–105

Li ZY, Zhang ZY, Emery T, Scherer A, Psaltis D (2006) Single mode optofluidic distributed feedback dye laser. Opt Express 14:696–701

Lim JM, Kim SH, Choi JH, Yang SM (2008) Fluorescent liquid-core/aircladding waveguides towards integrated optofluidic light sources. Lab Chip 8:1580–1585

Lopez CA, Lee CC, Hirsa AH (2005) Electrochemically activated adaptive liquid lens. Appl Phys Lett 87:134102

Mao X, Waldeisen JR, Juluri BK, Huang TJ (2007) Hydrodynamically tunable optofluidic cylindrical microlens. Lab Chip 7:1303–1308

Mao X, Lin SCS, Dong C, Huang TJ (2009a) Single-layer planar on-chip flow cytometer using microfluidic drifting based three-dimensional (3D) hydrodynamic focusing. Lab Chip 9:1583–1589

Mao X, Lin SCS, Lapsley MI, Shi J, Juluri BK, Huang TJ (2009b) Tunable liquid gradient refractive index (L-GRIN) lens with two degrees of freedom. Lab Chip 9:2050–2058

Miccio L, Finizio A, Grilli S, Vespini V, Paturzo M, Nicola DS, Ferraro P (2009a) Tunable liquid microlens arrays in electrodeless configuration and their accurate characterization by interference microscopy. Opt Express 17:2487–2499

Miccio L, Paturzo M, Grilli S, Vespini V, Ferraro P (2009b) Hemicylindrical and toroidal liquid microlens formed by pyroelectro-wetting. Opt Lett 34:1075–1077

Monneret S, Belloni F, Soppera O (2007) Combining fluidic reservoirs and optical tweezers to control beads/living cells contacts. Microfluid Nanofluid 3:645–652

Pang L, Levy U, Campbell K, Groisman A, Fainman Y (2004) Set of two orthogonal adaptive cylindrical lenses in a monolith elastomer device. Opt Express 13:9003–9013

Psaltis D, Quake SR, Yang C (2006) Developing optofluidic technology through the fusion of microfluidics and optics. Nature 442:381–386

Ren H, Wu ST (2007) Variable-focus liquid lens. Opt Express 15:5931–5936

Rosenauer M, Vellekoop MJ (2009) 3D fluidic lens shaping—a multiconvex hydrodynamically adjustable optofluidic microlens. Lab Chip 9:1040–1042

Schmidt H, Hawkins AR (2008) Optofluidic waveguides: I. Concepts and implementations. Microfluid Nanofluid 4:3–16

Seow YC, Liu AQ, Chin LK, Li XC, Huang HJ, Cheng TH, Zhou XQ (2008) Different curvature of tunable liquid microlens via the control of laminar flow rate. Appl Phys Lett 93:084101

Shi J, Hsiao VKS, Huang TJ (2007) Nanoporous polymeric transmission gratings for high-speed humidity sensing. Nanotechnology 18:465501

Shi J, Hsiao VKS, Walker TR, Huang TJ (2008a) Humidity sensing based on nanoporous polymeric photonic crystals. Sens Actuators B Chem 129:391–396

Shi J, Mao X, Ahmed D, Colletti A, Huang TJ (2008b) Focusing microparticles in a microfluidic channel with standing surface acoustic waves (SSAW). Lab Chip 8:221–223

Shi J, Ahmed D, Mao X, Lin SCS, Huang TJ (2009a) Acoustic tweezers: patterning cells and microparticles using standing surface acoustic waves (SSAW). Lab Chip 9:2890–2895

Shi J, Huang H, Stratton Z, Lawit A, Huang Y, Huang TJ (2009b) Continuous particle separation in a microfluidic channel via standing surface acoustic waves (SSAW). Lab Chip 9:3354–3359

Shopova SI, Zhou H, Fan X, Zhang P (2007) Optofluidic ring resonator based dye laser. Appl Phys Lett 90:221101

Sinton D, Erickson D, Li D (2003) Micro-bubble lensing induced photobleaching (m-BLIP) with application to microflow visualization. Exp Fluids 35:178–187

Song C, Nguyen NT, Tan SH, Asundi AK (2009) Modelling and optimization of micro optofluidic lenses. Lab Chip 9:1178–1184

Tang SKY, Stan CA, Whitesides GM (2008) Dynamically reconfigurable liquidcore liquid-cladding lens in a microfluidic channel. Lab Chip 8:395–401

Tovar AR, Lee AP (2009) Lateral cavity acoustic transducer. Lab Chip 9:41–43

Wang MM, Tu E, Raymond DE, Yang JM, Zhang H, Hagen N, Dees B, Mercer EM, Forster AH, Kariv I, Marchand PJ, Butler WF (2005) Microfluidic sorting of mammalian cells by optical force switching. Nat Biotechnol 23:83–87

Wolfe DB, Conroy RS, Garstecki P, Mayers BT, Fischbach MA, Paul KE, Prentiss M, Whitesides GM (2004) Dynamic control of liquid-core/liquid-cladding optical waveguides. Proc Natl Acad Sci USA 34:12434–12438

Wu J, Cui X, Lee LM, Yang C (2008) The application of Fresnel zone plate based projection in optofluidic microscopy. Opt Express 16:15595–15602

Xia YN, Whitesides GM (1998) Soft lithography. Ann Rev Mater Sci 28:153–184

Yang AHJ, Moore SD, Schmidt BS, Klug M, Lipson M, Erickson D (2009) Optical manipulation of nanoparticles and biomolecules in sub-wavelength slot waveguides. Nature 457:71–75

Yin D, Lunt EJ, Rudenko MI, Deamer DW, Hawkins AR, Schmidt H (2007) Planar optofluidic chip for single particle detection, manipulation, and analysis. Lab Chip 7:1171–1175

Zhang DY, Lien V, Berdichevsky Y, Choi J, Lo YH (2003) Fluidic adaptive lens with high focal length tenability. Appl Phys Lett 82:3171–3172

Zourob M, Mohr S, Brown BJT, Fielden PR, McDonnell MB, Goddard NJ (2005) An integrated optical leaky waveguide sensor with electrically induced concentration system for the detection of bacteria. Lab Chip 5:1360–1365